DENTAL MATERIALS 38 (2022) 204–213

Available online at www.sciencedirect.com

ScienceDirect

journal homepage: www.elsevier.com/locate/dental

Fatigue analysis of restored teeth longitudinally cracked under cyclic loading

Fei Lin[a], *Ronald Ordinola-Zapata*[c], *Ning Ye*[b,d], *Haiping Xu*[e], *Alex S.L. Fok*[b,*]

[a] *Department of Cariology and Endodontology, Peking University School and Hospital of Stomatology, Beijing 100081, China*

[b] *Minnesota Dental Research Center for Biomaterials and Biomechanics, School of Dentistry, University of Minnesota, Minneapolis, MN, 55455, USA*

[c] *Division of Endodontics, Department of Restorative Sciences, School of Dentistry, University of Minnesota, Minneapolis, MN, 55455, USA*

[d] *Department of Mechanical Engineering, College of Science and Engineering, University of Minnesota, Minneapolis, MN, 55455, USA*

[e] *Department of Stomatology, Affiliated Hospital of Qingdao University, Qingdao University, Qingdao 266003, China*

ARTICLE INFO

Article history:
Received 7 August 2021
Received in revised form
10 November 2021
Accepted 8 December 2021

Keywords:
Longitudinal crack
Cyclic loading
Fatigue analysis
Finite element analysis
Debonding

ABSTRACT

Objective: To investigate the fatigue behavior of restored teeth, in particular the mechanisms of longitudinal dentinal cracking under cyclic mechanical loading, using finite element analysis (FEA) and the stress-life (S-N) approach.

Methods: Ten root-filled premolars restored with resin composites were subjected to step-stress cyclic loading to produce longitudinal cracks. Fracture loads and number of cycles completed at each load level were recorded. FEA was used to predict the stress amplitude of each component under the global cyclic load. Both intact and debonded conditions were considered for the dentin-composite interface in the FEA. The predicted stress concentrations were compared with the fracture patterns to help elucidate the failure mechanisms. The S-N approach was further used to predict the lifetimes of the different components in the restored teeth. Cumulative fatigue damage was represented by the sum of the fractions of life spent under the different stress amplitudes.

Results: Longitudinal cracks were seen in ~50% of the samples with a mean fracture load of 770 ± 45 N and a mean number of cycles to failure of 32,297 ± 12,624. The longitudinal dentinal cracks seemed to start near the line angle of the cavity, and propagated longitudinally towards the root. The sum of fractions of life spent for the dentin-composite interface exceeded 1 after ~7000 cycles when that for dentin was much lower than 1, indicating that interfacial debonding would occur prior to dentin fracture. This was supported by micro-CT images showing widened interfacial space in the cracked samples. In the debonded tooth, FEA showed dentinal stress concentrations at the gingival wall of the

* Correspondence to: Minnesota Dental Research Center for Biomaterials and Biomechanics, 16-212 Moos Health Science Tower, 515 Delaware Street S.E., Minneapolis, MN 55455, USA.
E-mail address: alexfok@umn.edu (A.S.L. Fok).

https://doi.org/10.1016/j.dental.2021.12.005

cavity, which coincided with the longitudinal cracks found in the cyclic loading test. The sum of fractions of life spent for dentin was close to 1 at ~30,000 cycles, similar to the experimental value.

Significance: Debonding of the dentin-composite interface may occur prior to longitudinal cracking of dentin in root-filled teeth under cyclic loading. The approximate time of occurrence for these events could be estimated using fatigue analysis with stresses provided by FEA. This methodology can therefore be used to evaluate the longevity of restoration designs for root-filled teeth.

1. Introduction

Longitudinal cracks in endodontically-restored teeth extend vertically from the crown over time [1]. They may lead to biting pain, hypersensitivity, pulpitis, periodontal disease or even the loss of teeth [2,3]. Being able to produce longitudinal cracks in the laboratory will help us better assess the different restorative techniques. Compared with other methods of producing longitudinal cracks (e.g. thermal shocks), mechanical fatigue is more representative of the mastication process, which is considered to be an important etiology for longitudinal cracks [2,4,5]. We have successfully produced longitudinal cracks, using the step-stress cyclic-loading method, in root-filled teeth [6]. However, the mechanisms of initiation and propagation of the longitudinal cracks were still unclear. To shed light on these mechanisms, stress and fatigue analysis need to be performed.

A common method for evaluating the fatigue behavior of a material is to use the stress-life (S-N) curve, i.e., the relationship between the cyclic stress amplitude and the number of cycles to failure [7]. There have been several S-N studies on the fatigue behaviors of dental materials, e.g. dentin [8,9] and its interface with resin composites [10–13]. However, very few studies have utilized this approach to analyze a restored tooth with multiple materials [14]. One reason is that the stress amplitude of each component under cyclic loading is difficult to determine due to the complex anatomy of a restored tooth. Another reason is that different components display different S-N curves, many of which are still unknown [5]. Thus, to study the mechanisms of longitudinal cracking in restored teeth under cyclic loading, one must first establish the stress of each component as well as their S-N curves.

Finite element analysis (FEA) is a common method of evaluating the stress distributions of a structure [15]. The results could help establish the origin of failure since failure of a structure often initiates from sites of stress concentration [16]. In dentistry, FEA has been conducted in many studies to assess the stress distributions of restored teeth using 3D models constructed from micro-computed tomographic (micro-CT) images [17–20]. The stresses acquired from FEA could then be utilized in conjunction with the materials' S-N curves to determine their respective times to failure. Obviously, some components will fail before the others but gross failure of a restored tooth may not happen until one of the major load-bearing components has failed.

The aim of this study was to investigate the fatigue behavior of restored teeth, in particular the mechanisms of longitudinal dentinal cracking under cyclic mechanical loading using the S-N approach.

2. Methods

2.1. Tooth preparation and cyclic loading test

The tooth-preparation methods were the same as those reported previously [6]. Briefly, 10 freshly-extracted single-rooted mandibular premolars were prepared with standardized mesial-occlusal-distal (MOD) cavities and access cavities. The protocol (no. STUDY00010231) was approved by the Institutional Review Board of the University of Minnesota. Each tooth was treated with root canal therapy and restored with a fiber-post and resin composite. The roots of the restored teeth were coated with ~0.2-mm thick polyvinylsiloxane impression material (3M Express VPS, 3M ESPE) to simulate the periodontal ligament and then potted with acrylic resin (Dentsply Caulk, Milford, DE, USA) to simulate the surrounding bone.

The specimens were scanned using micro-CT (HMX-XT 225, Nikon Metrology Inc., Brighton, MI, USA) with a 0.5-mm thick aluminum filter. The scan parameters used were: 20-μm isotropic resolution, 115-kV accelerating voltage, 90-μA tube current, 720 projections, 4 frames/projection, and 708-ms exposure time. The 3D structures were reconstructed with the software CT Pro 3D XT 3.1.11 (Nikon Metrology Inc., Brighton, MI, USA) and visualized with VGSTUDIO MAX 3.1 (Volume Graphics GmbH, Heidelberg, Germany).

Cyclic mechanical loading of the specimens was conducted using the same method as described previously [6]. Specifically, the step-stress method was used with sinusoidal cycles at 1 Hz (Table 1). Fracture was determined from a sudden increase in stroke. The numbers of cycles to failure and the fracture loads were recorded.

2.2. Lifetime prediction using the S-N approach

A widely-used S-N model for predicting the fatigue lifetime of a material or structure is that due to Basquin [21]. It could be written as:

$$\sigma = A \cdot N^{B} \quad (1)$$

where σ is the cyclic stress amplitude, N is the number of cycles to failure, and A and B are the fatigue-life coefficient and exponent, respectively. The constants A and B for dentin

Table 1 – The maximum load and corresponding number of cycles for each load level. The minimum load is 0 throughout.

The maximum load (N)	Number of cycles
100	1000
200	1000
300	1000
400	3000
450	3000
500	3000
550	3000
600	3000
650	3000
700	3000
750	3000
800	3000
850	Until fracture

Table 2 – Fatigue parameters for dentin and dentin-composite interface.

	A (MPa)	B
Dentin [8]	114	-0.06
Dentin-composite interface [12]	15.12	-0.12

and the dentin-composite interface could be obtained from the literature (Table 2) [8,12]. Substituting them into Eq. (1) gives

$$\sigma_D = 114(N_D)^{(-0.06)} \quad (2)$$

$$\sigma_I = 15.12(N_I)^{(-0.12)} \quad (3)$$

where the subscripts D and I represent dentin and the dentin-composite interface, respectively.

Eqs. (2) and (3) can be rewritten as:

$$N_D = \sqrt[0.06]{\frac{114}{\sigma_D}} \quad (4)$$

$$N_I = \sqrt[0.12]{\frac{15.12}{\sigma_I}} \quad (5)$$

2.3. FEA

FEA was used to predict the stress amplitude of each component within the restored tooth under the global cyclic load. A 3D finite element model (Fig. 1) was generated from the micro-CT images of one of the samples using the software Mimics Research 19.0 (Materialise, Leuven, Belgium) and 3-Matic Research 11.0 (Materialise, Leuven, Belgium). The acrylic resin surrounding the root of the tooth to simulate the alveolar bone was also modeled. Uniform surface meshes and isoparametric tetrahedral elements with increasing mesh densities were used until convergence was achieved. The models were imported into the software Abaqus/CAE 2019 (SIMULIA, Dassault Systèmes, Johnston, RI, USA) for stress analysis. There were 22,395 nodes and 94,504 elements in the converged model. All the materials, except gutta-percha, were assumed to be homogeneous, isotropic and linearly elastic (Table 3). The gutta-percha was neglected since its Young's modulus was much lower than those of other materials; its inclusion may lead to compatibility problems for the analysis. The following two interfacial conditions were considered:

- 1) No debonding: Perfect bonding was assumed among all the materials; and
- 2) Debonding at the dentin-composite interface: Perfect bonding was assumed among all the materials except at the dentin-composite interface. The interaction between dentin and resin composite was set as frictionless contact to simulate debonding at the interface.

The second interfacial condition was considered to examine the effect of interfacial debonding on the stresses in the remaining components.

The bottom surface of the cylindrical "bone" block was fully constrained. The tooth was loaded vertically at the center of the occlusal surface via a 2-mm diameter stainless-steel sphere. The frictional coefficient between the sphere and the tooth was set at 0.3. Stress results were obtained for the different load levels used in the experiments (Table 1). The maximum principal stress and von Mises stress distributions were used to predict the possible origin of failure. Considering the viscoelastic and plastic behavior of dentin at high stresses, the peak value of von Mises stress was selected as σ_D at each load level [22,23]. σ_I was an effective stress calculated from the square root of the sum of the squares of the interfacial normal and shear stresses, since both of them were expected to contribute to debonding. Compressive normal stresses, however, were ignored. The corresponding predicted numbers of cycles to failure, N_D and N_I, were calculated by using Eqs. (4) and (5).

2.4. Failure prediction using cumulative fatigue damage

Since the step-stress method was used in the cyclic loading test, the damage caused by each load step needed to be calculated. The cumulative fatigue damage could then be given by the sum of the fractions of life spent under the different stress amplitudes as [24]:

$$\sum_{i=1}^{h} \frac{n_i}{N_i} \quad (6)$$

where h is the total number of stress levels, n_i is the number of cycles conducted at the stress amplitude σ_i, and N_i is the number of cycles to failure at σ_i. Failure would occur when the sum of the fractions of life spent exceeds unity [24].

2.5. Failure probability calculation

The failure probability distribution of the restored teeth was calculated by the following equation [25,26]:

$$P_f = \frac{s}{t+1} \quad (7)$$

where s is the rank of a specimen within a total sample size of t, ranked in an ascending order according to the number of cycles to failure in the cyclic loading test. P_f would be compared directly with the cumulative fatigue damage in Eq. (6), as the greater the fatigue damage the greater the likelihood of failure.

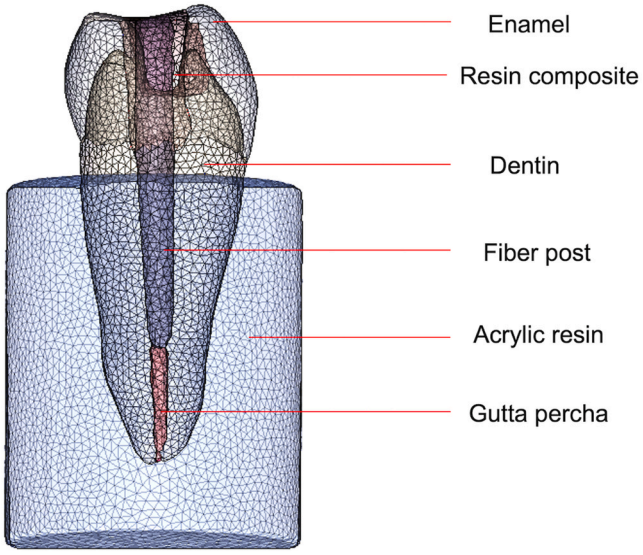

Fig. 1 – 3D finite element model of a sample specimen.

Table 3 – Assumed material properties for FEA.

Materials	Young's modulus (GPa)	Poisson's ratio
Dentin [35]	18.6	0.3
Enamel [36]	84.1	0.3
Resin composite [37]	12	0.3
Fiber post [38]	37	0.34
Gutta-percha [39]	0.14	0.49
Acrylic resin [40]	2.7	0.3

3. Results

3.1. *Fracture analysis*

Stable longitudinal cracks were seen in ~50% of the samples. The cracks seemed to start from the bottom of the cavity, near the line angle, and propagated longitudinally towards the root (Fig. 2b). Compared with the same sample before loading (Fig. 2a), it could be seen that the interfacial space between dentin and resin composite, initially occupied by the adhesive, became wider after cyclic loading. The mean fracture load and mean number of cycles to failure for longitudinally-cracked teeth were 770 ± 45 N and 32,297 ± 12,624, respectively.

The remaining samples failed with either unstable cuspal fractures (~20%, Fig. 2c) or mixed-mode fractures (~30%, Fig. 2d). The cracks in these samples tended to pass through the composite-dentin interface and propagated obliquely towards the outer surface of the crown or root (Fig. 2c, d). The mean fracture load and mean number of cycles to failure for these samples were 670 ± 71 N and 19,177 ± 8083, respectively, lower than those with stable longitudinal cracks.

3.2. *Stress distribution in fully-bonded restored tooth*

In the fully-bonded restored tooth under the maximum load of 800 N (Fig. 3a and d), the peak maximum principal stress of 1186 MPa was located at the occlusal surface around the loading point. High tensile stresses were also found in the fiber-post, dentin and enamel beneath the loading area. A peak tensile stress of ~15 MPa was predicted in the enamel along the enamel-dentin interface and that of ~20 MPa at the tip of the fiber-post. Within dentin, the high tensile stresses mainly occurred at the gingival wall of the MOD cavity, with a peak maximum principal stress of ~14 MPa. The peak von Mises stress in dentin of ~70 MPa, which was much higher than the peak tensile stress, was located at the pericervical area of the tooth. Note the similarity between the von Mises stress distribution and the crack paths of the samples. At the dentin-composite interface, normal tensile stresses of ~30 MPa could be seen at the mesial and distal side of the buccal/lingual wall of the cavity (Fig. 4b). Much higher interfacial shear stresses of ~80 MPa could be found at the lingual side of the cavity (Fig. 4c, d).

3.3. *Failure prediction for fully-bonded tooth*

We focused on interfacial debonding and dentin fracture, the main modes of failure seen experimentally. The high contact stresses at the loading point were ignored as they were numerical artefacts of the FEA which did not consider inelastic material behaviors such as yielding and micro-cracking. The expected lifetimes for dentin and the dentin-composite interface, i.e. N_D and N_I, at each load level were calculated using σ_D and σ_I determined by FEA, according to Eqs. (4) and (5) (Table 4). For dentin, the peak von Mises stress was used for calculation because of dentin's viscoelastic and plastic behavior at high stresses and the fact that its position corresponded well with the origin of dentin fracture. Also, the use of the peak tensile stress, the magnitude of which was much lower than that of the peak von Mises stress, grossly overestimated the time to failure. For the dentin-composite interface, the median value of the effective interfacial stress was used instead, since singular stresses existed at the edges

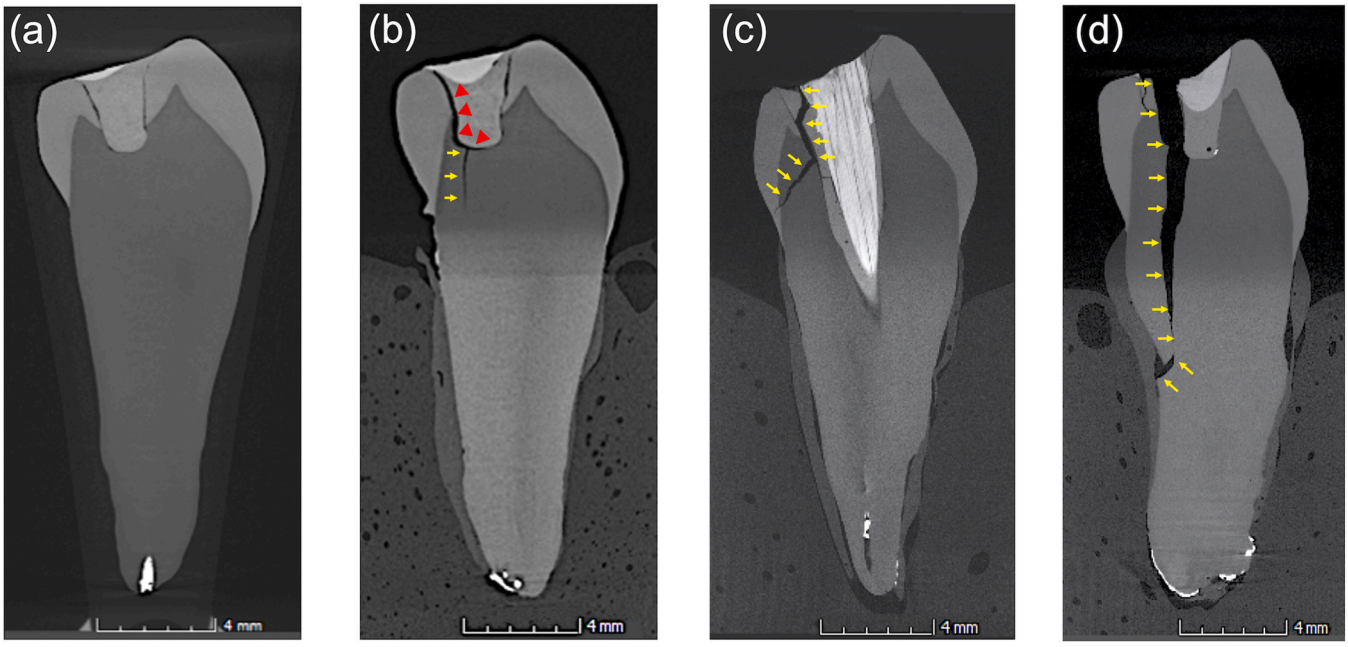

Fig. 2 – Micro-CT images before (a) and after (b, c, d) cyclic loading test. (a) and (b) show roughly the same section of the same sample before and after cyclic loading. (b), (c) and (d) show longitudinal, cuspal and mixed-mode fractures, respectively. The yellow arrows point to the positions of fractures. The red triangles indicate the widened dentin-composite interface after cyclic loading.

joining the different materials. Regardless, as the load increased, the stress amplitude increased while the corresponding number of cycles to failure decreased for both dentin and the dentin-composite interface. Under the same load, N_D was much higher than N_I. Thus, the interface was expected to fail before dentin.

Using n_i and N_i for each load level (Table 4), the sum of fractions of life spent for dentin and the dentin-composite interface was calculated using Eq. (6). These are plotted against the total number of cycles for the fully-bonded restored tooth in Fig. 5. For the dentin-composite interface, the fraction of life spent increased rapidly and exceeded 1 after ~7000 cycles, at which point the interface was expected to fail. For dentin, at the same number of cycles, the fraction of life spent was minimal, confirming that debonding of the dentin-composite interface would occur prior to dentin fracture. The applied load at which debonding was predicted to occur was 450 N (Table 4).

To confirm the above, micro-CT images of the longitudinally-cracked samples were compared with those of the same samples before loading (Fig. 2). It could be seen that the interfacial space between dentin and composite widened after cyclic loading, indicating debonding. In samples with cuspal or mixed-mode fractures, the dentin-composite interface formed part of the main crack, making it hard to ascertain whether debonding had happened prior to fracture.

3.4. *Stress distribution in debonded tooth*

The stress distributions of the debonded tooth at a load of 800 N are shown in Fig. 3b and e. The peak maximum principal stress near the loading area of 1205 MPa was ignored as explained above. Within dentin, the peak maximum principal stress was again found at the gingival wall of the cavity but had an increased value of ~35 MPa. Von Mises stress of ~50 MPa was also present at the gingival wall of the cavity (Fig. 3b). A stress concentration of ~30 MPa could be seen near the orifice of the root canal (Fig. 3b), which was not found in the fully-bonded restored tooth (Fig. 3a). The positions of the stress concentrations at the gingival wall of the cavity (Fig. 3b and e) again coincided with those of the longitudinal cracks seen in the cyclic loading test (Fig. 3c and f).

Resolving these concentrated stresses of dentin at the bottom of the cavity (Fig. 6a) into their orthogonal components (Fig. 6b–d) showed that it was the buccolingual component that contributed most to longitudinal cracking.

3.5. *Prediction of dentin fracture for debonded tooth*

The stress causing dentin fracture in the debonded tooth (σ_D') was determined from the FEA for occlusal loads higher than 450 N, the load at which debonding was predicted. The corresponding number of cycles to failure (N_D') was again calculated by using Eq. (4) (Table 5). Similar to the fully-bonded restored tooth, as the load increased, σ_D' increased while N_D' decreased. At loads lower than 450 N, σ_D and N_D from the fully-bonded restored tooth still applied.

Again, the sum of fractions of life spent for dentin over the different stress levels was calculated using Eq. (6) to estimate the cumulative fatigue damage to dentin. The resulting total fraction of life spent against the total number of cycles is plotted in Fig. 5. It can be seen that, compared to the fully-

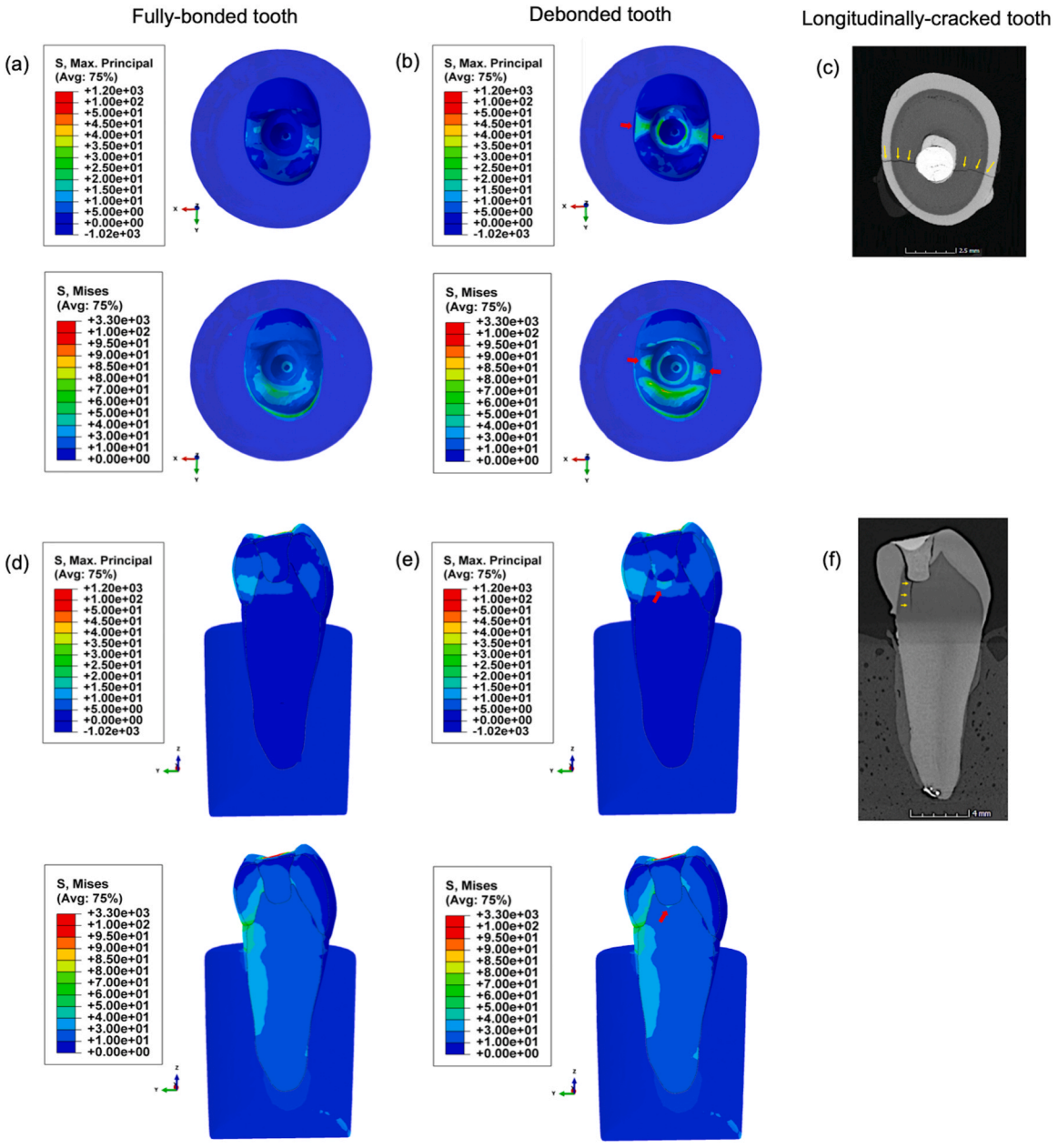

Fig. 3 – Comparison of maximum principal stress and von Mises stress distributions of fully-bonded tooth (a, d) and debonded tooth (b, e) with crack positions in a longitudinally-cracked tooth from the cyclic loading test (c, f). (a–c) are the top views while (d–f) are the sectional views. The red arrows point to the stress concentrations in dentin. The yellow arrows point to the positions of longitudinal cracks.

bonded tooth, damage to the dentin in the debonded tooth was predicted to accumulate more rapidly. The fraction of life spent was very low before 15,000 cycles. However, it then increased rapidly after 18,000 cycles and exceeded 1 at ~20,000 cycles.

The failure probability of the samples was also plotted against the number of cycles in Fig. 5 for comparison with the cumulative fatigue damage curves. The bulk of the experimental data lie within the predicted failure curves for interfacial debonding and dentin fracture. The first failure occurred at ~10,000 cycles, shortly after debonding was predicted, and the proportion of failure increased sharply at ~25,000 cycles, when dentin fracture was predicted to occur. There was thus good agreement between theory and experiment.

4. Discussion

To the best of our knowledge, very limited in vitro studies have successfully produced consistent longitudinal cracks in root-filled teeth such as those found clinically. We have recently succeeded in doing so in the laboratory by using the step-stress cyclic loading method [6]. However, the

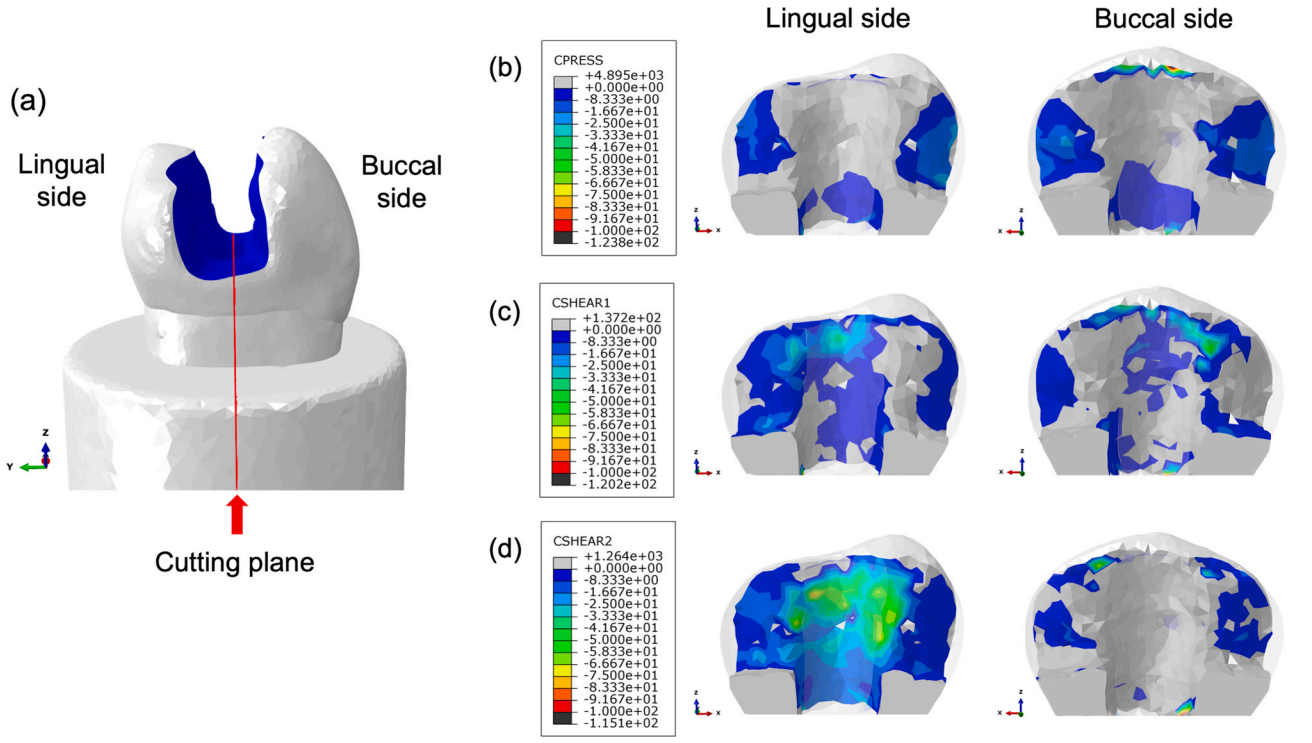

Fig. 4 – Interfacial normal stress (b) and shear stress (c, d) distributions from lingual and buccal sides of the fully-bonded tooth. (a) shows the cutting plane of the tooth.

Table 4 – Predicted stress and number of cycles to failure at each load level for dentin and dentin-composite interface of fully-bonded restored tooth.

i	Load (N)	n_i	Dentin			Dentin-composite interface		
			σ_D (MPa)	N_D	$\sum_{i=1}^{h} \frac{n_i}{N_i}$	σ_I (MPa)	N_I	$\sum_{i=1}^{h} \frac{n_i}{N_i}$
1	100	1000	8.78	3.60E+18	2.79E-16	1.31	7.32E+08	1.37E-06
2	200	1000	17.56	3.46E+13	2.90E-11	2.61	2.27E+06	4.40E-04
3	300	1000	26.35	4.00E+10	2.49E-08	3.92	7.74E+04	1.29E-02
4	400	3000	35.13	3.31E+08	9.04E-06	5.22	7.04E+03	4.26E-01
5	450	3000	39.52	4.66E+07	6.44E-05	5.88	2.64E+03	1.14E+00
6	500	3000	43.91	8.05E+06	3.73E-04	6.53	1.10E+03	2.74E+00
7	550	3000	48.30	1.64E+06	1.83E-03	7.18	4.95E+02	6.06E+00
8	600	3000	52.69	3.86E+05	7.79E-03	7.84	2.40E+02	1.25E+01
9	650	3000	57.09	1.01E+05	2.97E-02	8.49	1.23E+02	2.44E+01
10	700	3000	61.48	2.95E+04	1.02E-01	9.14	6.64E+01	4.52E+01
11	750	3000	65.87	9.34E+03	3.21E-01	9.79	3.74E+01	8.03E+01
12	800	3000	70.26	3.19E+03	3.13E+00	10.45	2.18E+01	4.58E+02
13	850	Until fracture	74.65	1.16E+03		11.10	1.32E+01	

mechanisms of initiation and propagation of longitudinal cracks under mechanical fatigue were still unclear. This study was therefore carried out to use a combination of FEA and the S-N approach to better understand the failure process.

A crack would initiate when the local stress exceeds the strength of the material or when the number of cycles exceeds its fatigue life [27]. The fatigue failure of root-filled teeth was predicted using Basquin's power law [21]. This method is commonly used to analyze the fatigue behavior of a single material or interface [7,9,11–13]. Indeed, the fatigue behaviors of dentin and the dentin-composite interface had been reported by other investigators [8,13], but this was the first time that such information was utilized to study the onset of longitudinal cracking in root-filled teeth. In our study, root-filled teeth, which are complex structures of multiple irregular components, were tested under clinically-relevant cyclic loading [6]. Each component possessed a different fatigue strength and was subjected to a different stress level (which needed to be determined using FEA) under the global load. As a result, some components would fail earlier than the others, and failure of the overall structure would be

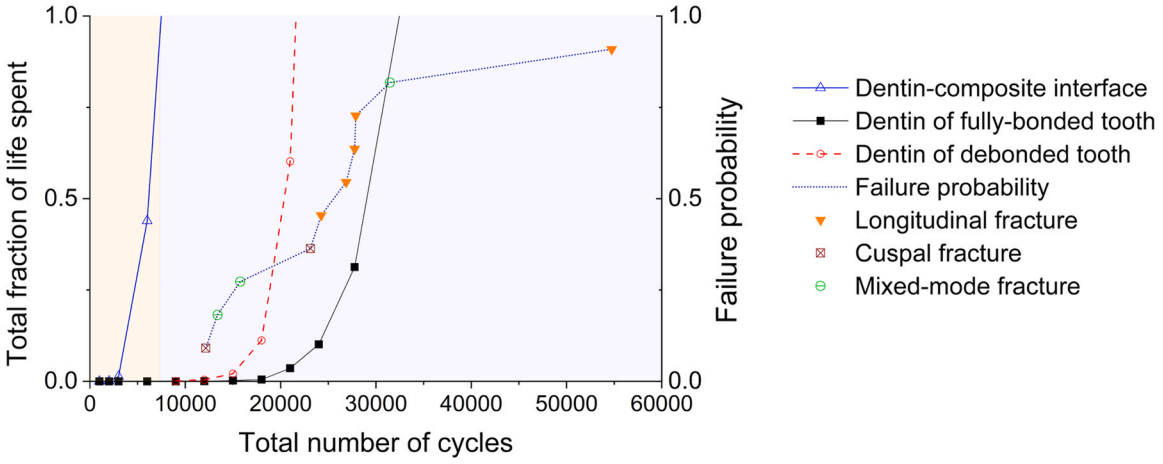

Fig. 5 – The predicted total fraction of life spent and experimental failure probability against total number of cycles for dentin and the dentin-composite interface in the fully-bonded and debonded restored tooth.

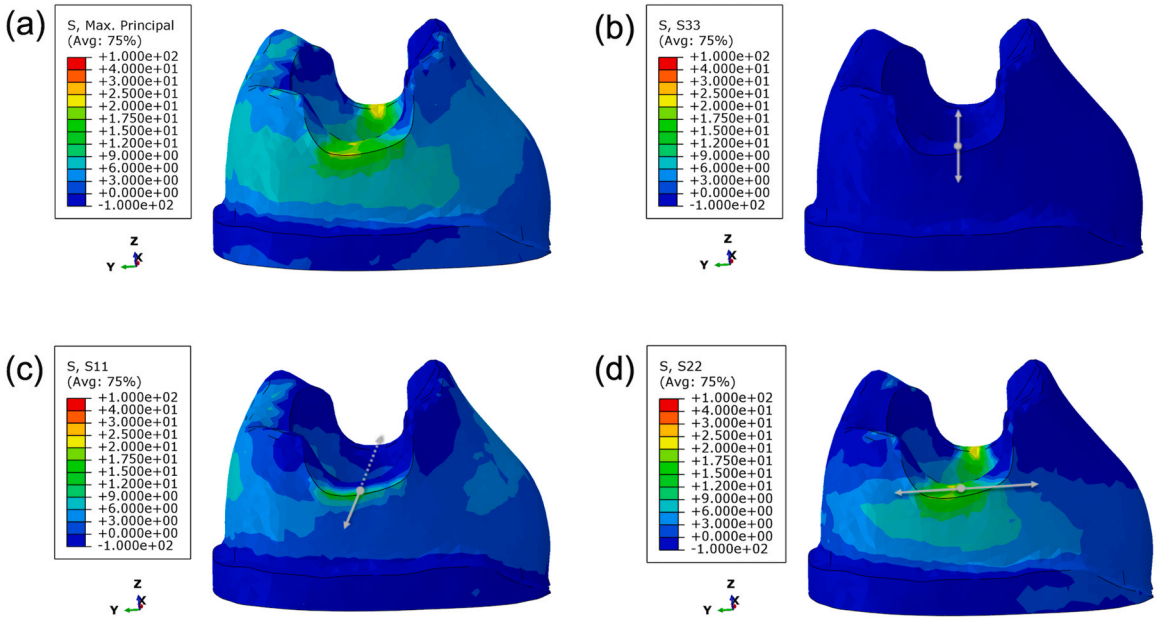

Fig. 6 – Distributions of maximum principal stress (a), stress in longitudinal direction (b), stress in mesiodistal direction (c), and stress in buccolingual direction (d) in dentin of debonded tooth. The gray arrows point to the direction of stress.

initiated by that of the component with the shortest life expectancy, which may not necessarily be the one with the highest stress [5].

We focused on the initiation of failure of dentin and the dentin-composite interface, and the order that they occurred. Those of enamel and the resin composite were ignored, despite the very high stresses predicted in these components near the loading point, because failure was not seen to have initiated from these components. Thus, the high contact stresses were assumed to have caused only local damage in these components that did not lead to gross failure. The analysis indicated that the dentin-composite interface failed before the bulk dentin. This was supported by micro-CT images which showed widening of the dentin-composite interface in samples with stable longitudinal cracks following cyclic loading. Indeed, gradual interfacial debonding may be a prerequisite and an important contributing factor for longitudinal cracking in root-filled teeth.

Debonding seemed to have started at the lingual side of the cavity, where high shear stress concentrations were predicted by FEA. The buccal and lingual cusps of lower premolars usually display different heights. This asymmetrical geometry might lead to bending of the tooth under mastication, which can shift the position of failure initiation to one side in addition to increasing the risk of debonding and cuspal fracture. Clinically, apart from mechanical stresses from mastication, the dentin-composite interface is also subjected to other challenges such as stresses from

Table 5 – Predicted stress and number of cycles to failure for dentin when debonding was considered.

	i	Load (N)	n_i	σ_D' (MPa)	N_D'	$\sum_{i=1}^{h} \frac{n_i}{N_i}$
Before debonding	1	100	1000	8.78	1.95E+16	2.79E-16
	2	200	1000	17.56	1.88E+11	2.90E-11
	3	300	1000	26.35	2.18E+08	2.50E-08
	4	400	3000	35.13	1.80E+06	9.05E-06
After debonding	5	450	3000	45.86	3.90E+06	7.69E-04
	6	500	3000	50.19	8.67E+05	3.46E-03
	7	550	3000	55.21	1.77E+05	1.69E-02
	8	600	3000	61.07	3.30E+04	9.10E-02
	9	650	3000	67.56	6.12E+03	4.90E-01
	10	700	3000	73.37	1.55E+03	1.94E+00
	11	750	3000	80.12	3.57E+02	8.40E+00
	12	800	3000	85.08	1.31E+02	7.62E+01
	13	850	Until fracture	91.96	3.59E+01	

polymerization shrinkage of the resin composite and corrosion due to degradative products from the saliva or biofilms [28,29]. Thus, debonding of the dentin-composite interface can often be observed in restored teeth in the form of marginal discoloration or secondary caries [30,31].

According to the S-N analysis, debonding began at ~7000 cycles when the load was 450 N. When completed, it was shown to redistribute the stresses, shifting the positions of stress concentration to the gingival wall of the MOD cavity where subcritical crack initiation and propagation in dentin subsequently occurred. Note that such stable crack growth cannot occur under static loading because of the large amount of elastic energy released in a very short time from the more rapid interfacial debonding [6].

Debonding also increased the stresses in dentin which would accelerate its fracture. The loss of bonding between the tooth and the composite means that one of the cusps would need to take up more of the load. As a result, the stresses at the gingival wall of the MOD cavity increased, as shown by the FEA. The positions of these stress concentrations coincided with initiation sites of longitudinal cracks in the fractured specimens. Whether cuspal fracture or stable crack growth occurred depended on the orientation of the initiated crack and the subsequent stress state. It should also be noted that debonding resulted in concentrated stresses uniformly distributed around the orifice of the root canal (Fig. 3b). This was probably due to increased loading to the root canal through the fiber post as a result of reduced support from the crown.

The direction of the peak stress determines the direction of crack initiation and propagation. Most of the cracks occurred in dentin are opening-mode cracks induced by tensile stresses at the locations of stress concentration [32]. The direction of the stress contributing to an opening-mode crack is perpendicular to that of crack propagation. The main stress producing the longitudinal cracks in our study was shown by FEA to be the circumferential tensile stress. This agrees with Krishnan et al. [33] who demonstrated that horizontal forces are the main cause of axial splitting of teeth. Clinically, longitudinal cracks in cracked teeth are vertically propagated and oriented mesiodistally [2], as those produced in our cyclic loading test. Thus, the stress inducing this type of cracks should be perpendicular to the mesiodistal directions of the tooth, i.e. in the buccolingual direction. This agrees with our FEA.

The good agreement between theory and experiment validated the S-N approach. However, the FEA was based on the geometry of one sample only. In reality, the samples varied in geometry as well as material properties, resulting in the variations seen in the load and number of cycles to failure. The predictions were also for failure initiation only, whereas in the experiments failure could only be detected when debonding or cracking reached an unsteady state. This may explain why the experimental numbers of cycles to failure were generally greater than those predicted. Ref. [34] provided an analysis of stable crack propagation in dentin. Clinically, the tooth stresses are lower than those produced by the step-stress method used in this study. Therefore, the number of cycles required to initiate and propagate the cracks would be much higher.

5. Conclusion

Debonding of the dentin-composite interface likely occurred prior to longitudinal cracking of dentin in root-filled teeth under cyclic loading. The approximate time of occurrence for these events could be estimated using fatigue analysis with stresses provided by FEA.

Acknowledgment

Research reported in this paper was supported by the National Institute of Dental and Craniofacial Research of the National Institutes of Health under award number R01DE027043. The content is solely the responsibility of the authors and does not necessarily represent the official views of the National Institutes of Health. This work was also supported by National Natural Science Foundation of China through a grant (No. 12102009) awarded to Fei Lin and a pre-K grant from the National Institutes of Health's National Center for Advancing Translational Sciences, UL1TR002494 (CTSI-UMN), awarded to Ronald Ordinola-Zapata. Fei Lin would also like to acknowledge Minnesota Dental Research Center for Biomaterials and Biomechanics for the financial support with a Key Opinion Leaders Scholarship sponsored by 3Mgives.

REFERENCES

[1] Rivera EM, Walton RE. Cracking the cracked tooth code: detection and treatment of various longitudinal tooth fractures. Endod Colleagues Excell 2008:2–7.
[2] Rivera EM, Walton RE. Longitudinal tooth fractures: findings that contribute to complex endodontic diagnoses. Endod Top 2007;16:82–111.
[3] Lubisich EB, Hilton TJ, Ferracane J. Cracked teeth: a review of the literature. J Esthet Restor Dent 2010;22:158–67.
[4] Banerji S, Mehta SB, Millar BJ. Cracked tooth syndrome. Part 1: aetiology and diagnosis. Br Dent J 2010;208:459–63.
[5] Ordinola-Zapata R, Fok ASL. Research that matters: debunking the myth of the "fracture resistance" of root filled teeth. Int Endod J 2021;54:297–300.
[6] Lin F, Ordinola-Zapata R, Xu H, Heo YC, Fok A. Laboratory simulation of longitudinally cracked teeth using the step-stress cyclic loading method. Int Endod J 2021;54:1638–46.
[7] Arola D. Fatigue testing of biomaterials and their interfaces. Dent Mater 2017;33:367–81.
[8] Mutluay MM, Yahyazadehfar M, Ryou H, Majd H, Do D, Arola D. Fatigue of the resin-dentin interface: a new approach for evaluating the durability of dentin bonds. Dent Mater 2013;29:437–49.
[9] Yahyazadehfar M, Mutluay MM, Majd H, Ryou H, Arola D. Fatigue of the resin-enamel bonded interface and the mechanisms of failure. J Mech Behav Biomed Mater 2013;21:121–32.
[10] Li K, Guo J, Li Y, Heo YC, Chen J, Xin H, et al. Accelerated fatigue testing of dentin-composite bond with continuously increasing load. Dent Mater 2017;33:681–9.
[11] Orrego S, Melo MA, Lee SH, Xu HHK, Arola DD. Fatigue of human dentin by cyclic loading and during oral biofilm challenge. J Biomed Mater Res – Part B Appl Biomater 2017;105:1978–85.
[12] Li Y, Carrera C, Chen R, Li J, Chen Y, Lenton P, et al. Fatigue failure of dentin-composite disks subjected to cyclic diametral compression. Dent Mater 2015;31:778–88.
[13] Zhang Z, Beitzel D, Mutluay M, Tay FR, Pashley DH, Arola D. On the durability of resin-dentin bonds: identifying the weakest links. Dent Mater 2015;31:1109–18.
[14] Homaei E, Jin XZ, Pow EHN, Matinlinna JP, Tsoi JKH, Farhangdoost K. Numerical fatigue analysis of premolars restored by CAD/CAM ceramic crowns. Dent Mater 2018;34:e149–57.
[15] Munari LS, Bowles WR, Fok ASL. Relationship between canal enlargement and fracture load of root dentin sections. Dent Mater 2019;35:818–24.
[16] Singh V, Misra A, Marangos O, Park J, Ye Q, Kieweg SL, et al. Fatigue life prediction of dentin-adhesive interface using micromechanical stress analysis. Dent Mater 2011;27:e187–95.
[17] Ausiello P, Ciaramella S, Martorelli M, Lanzotti A, Zarone F, Watts DC, et al. Mechanical behavior of endodontically restored canine teeth: effects of ferrule, post material and shape. Dent Mater 2017;33:1466–72.
[18] Chang YH, Wang HW, Lin PH, Lin CL. Evaluation of early resin luting cement damage induced by voids around a circular fiber post in a root canal treated premolar by integrating micro-CT, finite element analysis and fatigue testing. Dent Mater 2018;34:1082–8.
[19] Xiong Y, Huang SH, Shinno Y, Furuya Y, Imazato S, Fok A, et al. The use of a fiber sleeve to improve fracture strength of pulpless teeth with flared root canals. Dent Mater 2015;31:1427–34.
[20] Askerbeyli Örs S, Aksel H, Küçükkaya Eren S, Serper A. Effect of perforation size and furcal lesion on stress distribution in mandibular molars: a finite element analysis. Int Endod J 2019;52:377–84.
[21] Basquin OH. The exponential law of endurance tests. Proc Am Soc Test Mater 1910;10:625–30.
[22] Borodin EN, Seyedkavoosi S, Zaitsev D, Drach B, Mikaelyan KN, Panfilov PE, et al. Viscoelasticity and plasticity mechanisms of human dentin. Phys Solid State 2018;60:120–8.
[23] Zaytsev D, Ivashov AS, Mandra JV, Panfilov P. On the deformation behavior of human dentin under compression and bending. Mater Sci Eng C 2014;41:83–90.
[24] Benham PP, Crawford RJ, Armstrong CG. Mechanics of Engineering Materials. Addison-Wesley; 1996.
[25] Bergman B. On the estimation of the Weibull modulus. J Mater Sci Lett 1984;3:689–92.
[26] Quinn JB, Quinn GD. A practical and systematic review of Weibull statistics for reporting strengths of dental materials. Dent Mater 2010;26:135–47.
[27] Yahyazadehfar M, Ivancik J, Majd H, An B, Zhang D, Arola D. On the mechanics of fatigue and fracture in teeth. Appl Mech Rev 2014;66. (03080301–03080319).
[28] Aregawi WA, Fok ASL. Shrinkage stress and cuspal deflection in MOD restorations: analytical solutions and design guidelines. Dent Mater 2021;37:783–95.
[29] Rocca GT, Gregor L, Sandoval MJ, Krejci I, Dietschi D. In vitro evaluation of marginal and internal adaptation after occlusal stressing of indirect class II composite restorations with different resinous bases and interface treatments. "Post-fatigue adaptation of indirect composite restorations". Clin Oral Invest 2012;16:1385–93.
[30] Da Veiga AMA, Cunha AC, Ferreira DMTP, da Silva Fidalgo TK, Chianca TK, Reis KR, et al. Longevity of direct and indirect resin composite restorations in permanent posterior teeth: a systematic review and meta-analysis. J Dent 2016;54:1–12.
[31] Borgia E, Baron R, Borgia JL. Quality and survival of direct light-activated composite resin restorations in posterior teeth: a 5- to 20-year retrospective longitudinal study. J Prosthodont 2019;28:e195–203.
[32] Zhang D, Nazari A, Soappman M, Bajaj D, Arola D. Methods for examining the fatigue and fracture behavior of hard tissues. Exp Mech 2007;47:325–36.
[33] Krishnan U, Moule A, Michael S, Swain M. Fractographic analysis of a split tooth presenting radiographically as a horizontal root fracture in an unrestored mandibular second molar. J Endod 2018;44:304–11.
[34] Arola D, Huang MP, Sultan MB. The failure of amalgam dental restorations due to cyclic fatigue crack growth. J Mater Sci Mater Med 1999;10:319–27.
[35] Peyton FA, Mahler DB, Hershenov B. Physical properties of dentin. J. Dent. Res. 1952;31:366–70.
[36] Yettram AL, Wright KWJ, Pickard HM. Finite Element Stress Analysis of the Crowns of Normal and Restored Teeth. J. Dent. Res. 1976;55:1004–11.
[37] Sideridou I, Tserki V, Papanastasiou G. Study of water sorption, solubility and modulus of elasticity of light-cured dimethacrylate-based dental resins. Biomaterials 2003;24:655–65.
[38] Lassila LVJ, Tanner J, Le Bell AM, Narva K, Vallittu PK. Flexural properties of fiber reinforced root canal posts. Dent. Mater. 2004;20:29–36.
[39] Friedman CE, Sandrik JL, Heuer MA, Rapp GW. Composition and physical properties of gutta-percha endodontic filling materials. J. Endod. 1977;3:304–8.
[40] Suwannaroop P, Chaijareenont P, Koottathape N, Takahashi H, Arksornnukit M. In vitro wear resistance, hardness and elastic modulus of artificial denture teeth. Dent. Mater. J. 2011;30:461–8.